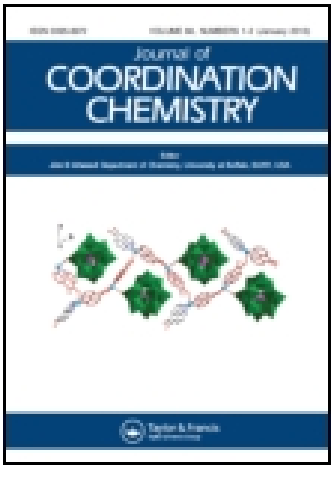

Journal of Coordination Chemistry
Publication details, including instructions for authors and subscription information:
http://www.tandfonline.com/loi/gcoo20

Effects of pyrene on the photophysical and two-photon absorption-based nonlinear optical properties of indium(III) phthalocyanines

Kayode Sanusi[a] & Tebello Nyokong[a]
[a] Department of Chemistry, Rhodes University, Grahamstown, South Africa

Accepted author version posted online: 28 Aug 2014.Published online: 23 Sep 2014.

Journal of Coordination Chemistry, 2014
Vol. 67, No. 17, 2911–2924, http://dx.doi.org/10.1080/00958972.2014.959509

Effects of pyrene on the photophysical and two-photon absorption-based nonlinear optical properties of indium(III) phthalocyanines

KAYODE SANUSI and TEBELLO NYOKONG*

Department of Chemistry, Rhodes University, Grahamstown, South Africa

(*Received 15 June 2014; accepted 29 July 2014*)

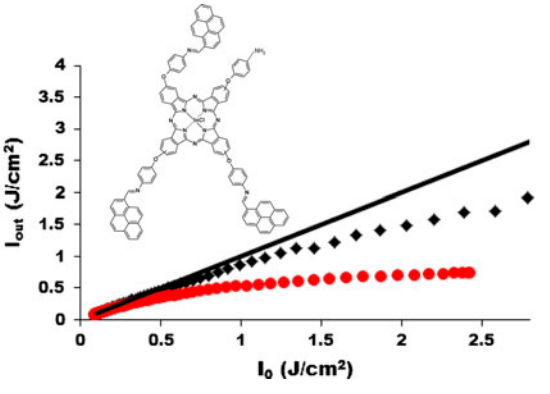

Photophysical and two-photon-dependent nonlinear absorption properties of two chloroindium(III) phthalocyanines bearing pyrene units have been investigated. The tetra- (**3**) and the tri- (**4**) pyrene-substituted phthalocyanines exhibit strong triplet absorption with high triplet yields (Φ_T) of 0.79 and 0.83, respectively. The measured nonlinear optical data, such as the two photon absorption cross-sections, the third- and second-order nonlinearities were found to be comparable with those of literature, thus, making the compounds promising candidates for a broad range of nonlinear optical applications.

Keywords: Indium phthalocyanine; Pyrene; Two-photon absorption; Limiting threshold; *Z*-scan; Nonlinear optics

1. Introduction

Metallophthalocyanines (MPcs) have been a subject of extensive study because of their diverse applications in areas such as dye-sensitized solar cells [1], photodynamic therapy of

*Corresponding author. Email: t.nyokong@ru.ac.za

cancer [2], electrocatalysis [3], optical sensors [4, 5], and nonlinear optics [6, 7]. Most of the properties exhibited by this family of compounds are dependent on their extensive delocalized 18π-electron systems which can bring about interesting photophysical properties [8, 9].

In the current work, we prepared from the previously reported tetraaminophenoxy indium (III) Pc (**1**) [10], tetra- (**3**) and tri- (**4**) substituted indium(III)-based phthalocyanines, bearing pyrene moieties (scheme 1). Phthalocyanines bearing pyrene substituents are known [11, 12], however, their nonlinear optical (NLO) behaviors have not yet been reported.

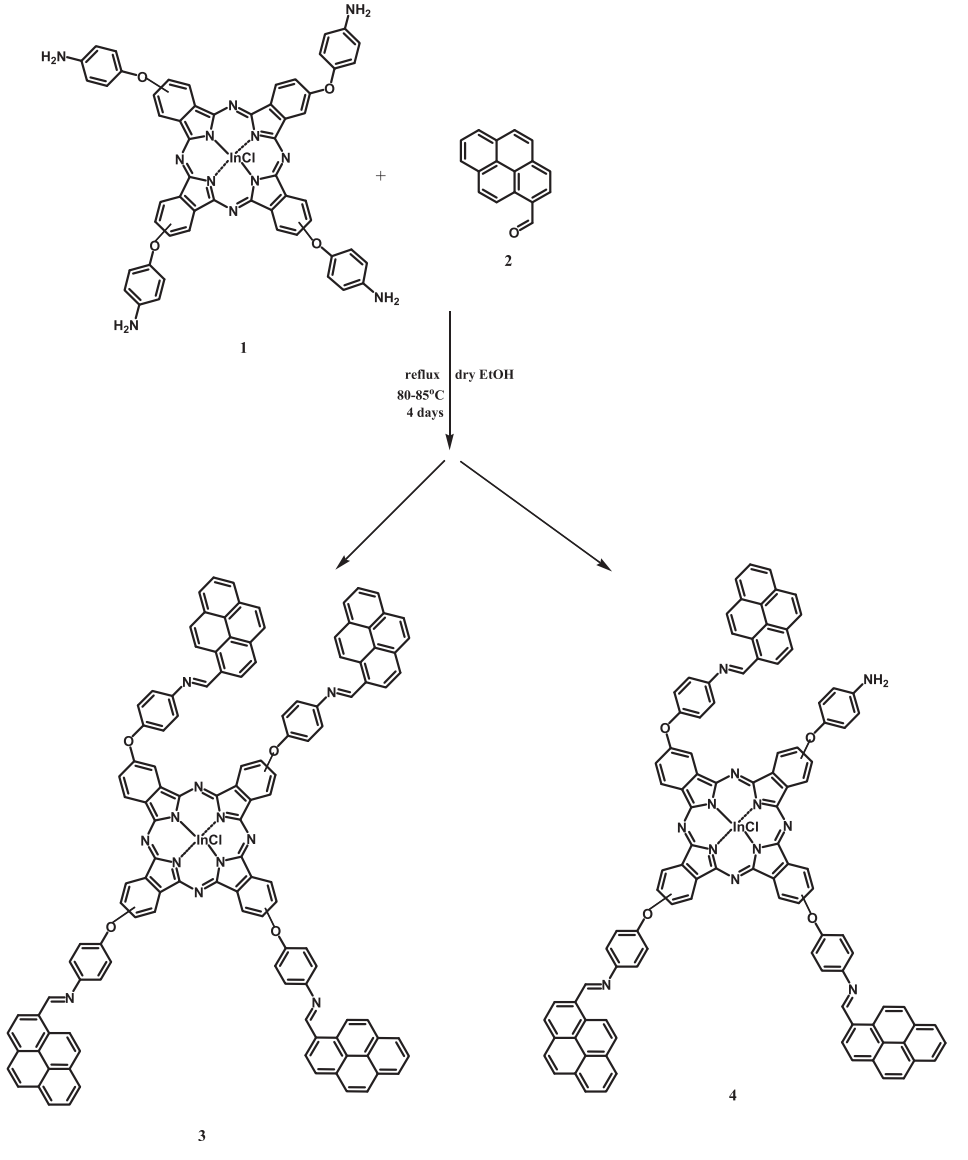

Scheme 1. Synthesis of pyrenophenoxy InPcs, **3** and **4**.

Improved photophysical properties of pyrene monosubstituted Zn phthalocyanine with an imine bridge separating the Pc ring and the pyrene moiety has been reported [13]. An improvement in photophysical properties is expected to result in enhanced NLO behavior. In **3** and **4**, the pyrene moieties are separated by phenoxy bridges. Owing to the higher number of pyrene moieties in the current Pcs compared to earlier reported pyrene monosubstituted Zn phthalocyanine, which has only one pyrene unit [13], significant enhancement in the photophysical properties than what was previously observed [13] is expected. A good understanding of the photophysical behaviors of these complexes, such as the singlet- and the triplet-state behaviors, would be useful in understanding their NLO properties. The past work showed the importance of asymmetry on the photophysical, photochemical, and optical limiting properties of phthalocyanines [13–15]. Hence in this work, we compared the NLO and the photophysical properties of symmetrical (**3**) and asymmetrical (**4**) pyrene-substituted indium(III) Pcs (scheme 1). Both Pcs possess heavy indium(III), thus giving an efficient intersystem crossing (ISC) from the singlet to the triplet state as a consequence of strong spin–orbit coupling [16, 17], which also improves their optical limiting properties [7, 18, 19]. Our aim, therefore, is to investigate the photophysical and nonlinear optical properties of these new phthalocyanine derivatives and compare the results with those of previously reported, **1** to show their relative suitability for applications in optical limiting.

2. Experimental

2.1. *Materials*

The synthesis of 2(3),9(10),16(17),23(24)-tetrakis-(4-aminophenoxy)-phthalocyaninato indium(III) chloride (**1**) has been reported [10]. Zinc phthalocyanine (ZnPc), spectroscopic dimethyl sulphoxide (DMSO), chloroform and pyrene-1-carboxaldehyde (**2**) were obtained from Sigma Aldrich. Deuterated DMSO-d_6 was obtained from Merck. Absolute ethanol (abs. EtOH), n-hexane, methanol (MeOH), and acetone were purchased from SAARCHEM. All solvents were of reagent grade and dried before use.

2.2. *Equipment*

Infrared spectra were collected on a Perkin-Elmer universal ATR sampling accessory spectrum 100 FT-IR spectrometer. ^{1}H NMR spectra were obtained using a Bruker AVANCE 600 MHz NMR spectrometer in DMSO-d_6. Elemental analyses were done using a Vario-Elementar Microcube ELIII, while mass spectral data were collected on a Bruker Auto-FLEX III Smart-beam TOF/TOF mass spectrometer using α-cyano-4-hydrocinnamic acid as the matrix in the positive ion mode.

All *Z*-scan experiments described in this study were performed using a frequency-doubled Nd : YAG laser (Quanta-Ray, 1.5 J/10 ns fwhm pulse duration) as the excitation source. The laser was operated in a near Gaussian transverse mode at 532 nm (second harmonic), with a pulse repetition rate of 10 Hz and energy range of 0.1 μJ–0.1 mJ, as limited by the energy detectors (Coherent J5-09). The low repetition rate of the laser prevents cumulative thermal nonlinearities. The beam was spatially filtered to remove the higher order modes and tightly focused with a 15 cm focal length lens. The *Z*-scan system size ($l \times w \times h$) used was 600 mm × 300 mm × 350 mm (excluding the computer, energy meter,

translation stage driver, and laser system). The liquid samples were placed in a cuvette (internal dimensions: 2 mm × 10 mm × 55 mm, 0.7 mL) and a path length of 2 mm (Starna 21-G-2).

The nanosecond laser flash photolysis set-up to investigate the excited-state properties comprised of coupled laser systems, a Nd-YAG laser (already described above) pumping Lambda-Physik FL3002 dye (Pyridin 1 dye in methanol) laser. The analyzing beam source was a Thermo Oriel 66902 xenon arc lamp. A Kratos Lis Projekte MLIS-X3 photomultiplier coupled with a monochromator allows for selective excitation at wavelengths between 400 and 850 nm when required. Signals were recorded with a two-channel, 300 MHz digital real time oscilloscope (Tektronix TDS 3032C).

Ground state electronic absorption spectra were recorded on a Shimadzu UV-2550 spectrophotometer. Fluorescence emission spectra were recorded on a Varian Eclipse spectrofluorimeter. Fluorescence decay times were measured using a time correlated single photon counting (TCSPC) technique (FluoTime 200, Picoquant GmbH). The excitation source was a diode laser (LDH-P-670 driven by PDL 800-B, 670 nm, 20 MHz repetition rate, 44 ps pulse width, Picoquant GmbH). The details of the set-up have been previously described [20].

2.3. *Synthesis*

2.3.1. 2(3),9(10),16(17),23(24)-Tetrakis-(4-((pyren-1-yl)methyleneamino)-phenoxy)-phthalocyaninato indium(III) chloride (3) (scheme 1). A mixture of **1** (0.10 g, 0.092 mmol) and **2** (0.094 g, 0.41 mmol) was refluxed in 3 mL dry EtOH at 80–85 °C under an inert atmosphere for 4 days. The crude product was cooled to room temperature and washed, respectively, in methanol, ethanol, n-hexane, and acetone by centrifugation, and was allowed to dry in air. The product was thereafter purified over a silica gel column using a DMF/EtOH mixture (2 : 1). Final purification of the compound was achieved by Soxhlet extraction using ethanol, water, and acetone in succession. The product was thereafter dried, ground, and characterized.

Complex **3** yield: (65%). UV–vis (DMSO): λ_{max}/nm (log ε): 697 (5.16), 627 (3.47), 369 (5.18). FT-IR [ATR (ν_{max}/cm^{-1})]: 3039, 2916, 2856 (C–H aromatic), 1668 (C=N imine), 1602, 1471 (C=C aromatic), 1222, 1195 (C–O–C), 945, 889, 822, 742, 714 (Pc-Skeleton). ^{1}H NMR (600 MHz, DMSO-d$_6$): δ ppm: 7.00–7.20 (8H, m, phenyl-H), 7.50–7.56 (2H, m, Pc-H), 8.10–8.25 (8H, m, phenyl-H), 8.27–8.30 (4H, m, Pc-H), 8.50–8.52 (4H, m, Pc-H), 8.63–8.68 (16H, m, pyr-H), 8.71–8.73 (8H, m, pyr-H), 8.75–8.78 (2H, m, Pc-H), 8.81–8.85 (8H, m, pyr-H), 8.87–8.90 (4H, d, pyr-H) 8.93–8.98 (4H, s, imine-H). Anal. Calcd for $C_{124}H_{68}N_{12}O_4ClIn$ (6H_2O): C, 72.71; H, 3.94; N, 8.21. Found: C, 71.94; H, 3.97; N, 8.12. MS (MALDI-TOF) *m/z:* Calcd 1938; Found: 1936 [M−2H]$^+$.

2.3.2. 2(3),9(10),16(17)-Trikis-(4-((pyren-1-yl)methyleneamino)phenoxy)-2(3)-amino-phenoxy phthalocyaninato indium(III) chloride (4) (scheme 1). The synthesis of **4** was as outlined for **3**, except that 0.060 g (0.26 mmol) of the pyrene (**2**) was employed for 0.10 g (0.092 mmol) of **1**. The fraction of interest was obtained following a systematic chromatographic separation using a 5 : 1 mixture of DMF/MeOH on a silica gel column. The final purification of this fraction was done following the method described for **3** above.

Complex **4** yield: (37%). UV–vis (DMSO): λ_{max}/nm (log ε): 699 (5.11), 632 (3.49), 365 (5.06). FT-IR [ATR (ν_{max}/cm^{-1})]: 3206 (N–H), 3043, 2922, 2856 (C–H aromatic), 1670 (C=N imine), 1604, 1497, 1473 (C=C aromatic), 1266, 1223, 1115 (C–O–C), 946, 890, 827, 742, 716, 681 (Pc-Skeleton). ^{1}H NMR (600 MHz, DMSO-d$_6$): δ ppm: 6.36–6.42 (2H, br. s, –NH$_2$), 7.11–7.14 (2H, m, phenyl-H), 7.18–7.21 (2H, m, phenyl-H), 7.32–7.38 (6H, m, phenyl-H), 7.41–7.47 (2H, m, Pc-H), 7.63–7.68 (4H, m, Pc-H), 7.72–7.87 (6H, m, phenyl-H), 7.89–8.19 (3H, m, Pc-H), 8.23–8.34 (12H, m, pyr-H), 8.38–8.44 (6H, m, pyr-H), 8.48–8.53 (3H, m, Pc-H), 8.57–8.63 (6H, m, pyr-H), 8.67–8.70 (3H, br. s, imine-H), 8.73–8.75 (3H, d, pyr-H). Anal. Calcd for $C_{107}H_{60}N_{12}O_4ClIn$ (4H$_2$O): C, 71.40; H, 3.81; N, 9.34. Found: C, 71.47; H, 3.35; N, 9.64. MS (MALDI-TOF) *m/z:* Calcd 1728; Found: 1730 $[M + 2H]^+$.

2.4. *Photophysical parameters*

Fluorescence (Φ_F) and triplet (Φ_T) quantum yields were determined in DMSO by the comparative methods described before [21–24] using ZnPc in DMSO as a standard. Φ_F = 0.2 [22] and Φ_T = 0.65 [24] for ZnPc standard in DMSO. Fluorescence emission spectra were obtained by exciting both the sample and standard at 610 nm. Triplet absorption and singlet depletion curves were observed at 400 μs time delay. To ensure the two samples and standard absorb the same amount of photons, the wavelength of the source laser beam was set at 680 nm, which is the position of intersection of the spectra of samples and standard, i.e. the λ at which they all have the same ground state absorption.

2.5. *Z-scan measurements*

The *Z*-scan experiment was performed according to the method described by Sheik-Bahae *et al.* [25–27]. Assuming a Gaussian spatial and temporal pulse, and using the open aperture (OA) *Z*-scan theory for multi-photon absorption (*n*PA) by Sutherland [28], the general equation for OA normalized transmittance can be written as [29],

$$T_{OA(2PA)} = \frac{1}{1 + \beta_2 L_{eff}(I_{00}/(1 + (z/z_0)^2))} \tag{1}$$

where I_{00} is the on-focus incident peak intensity, β_2 is the two photon absorption (2PA) coefficient, L_{eff}, z, and z_0 are the effective path length in the sample of length L, translation distance of the sample relative to the focus, and Rayleigh length, respectively. Rayleigh length is defined as $\pi w_o^2/\lambda$, where λ is the wavelength of the laser beam and w_0 is the beam diameter at the focus (z = 0). L_{eff} is given by equation (2):

$$L_{eff} = \frac{1 - e^{-\alpha L}}{\alpha} \tag{2}$$

where α is the linear absorption coefficient.

Equation (1) is an analytical expression for OA transmittance for two-photon absorbers, where other terms such as three-photon absorption are ignored. The good agreement between the experimental and theoretical 2PA transmittance was further substantiated by plotting $1/T$ (1/transmittance) *versus* I_0 (incident intensity), equation (3), which is a standard expression for a pure 2PA process in wavelength regions where there is no linear absorption [30, 31],

$$1/T = 1 + \beta_2 g^{(2)} I_0 L \tag{3}$$

where β_2 is the 2PA coefficient as defined above, $g^{(2)}$ is the degree of second-order coherence of the laser pulses, I_0 is the incident intensity, L is the sample path length, and T is the transmittance. The β_2 values are those obtained from the fittings using equation (1).

The molecular 2PA cross-section σ_2 (in units of $cm^4\,s\,photon^{-1}$) is calculated from the 2PA coefficient (β_2) using equation (4) [30]:

$$\sigma_2 = \frac{1000 h\upsilon \beta_2}{N_A C} \tag{4}$$

where N_A is the Avogadro number, C is the sample concentration, and $h\upsilon$ is the energy of an incident photon in joules.

The imaginary component of the third order susceptibility ($I_m[\chi^{(3)}]$) is given by equation (5) [32]:

$$I_m[\chi^{(3)}] = n^2 \varepsilon_0 c \lambda \beta_2 / 2\pi \tag{5}$$

where n and c are the linear refractive index and the speed of light, respectively, ε_0 is the permittivity of free space, λ, and β_2 terms are as described above.

Second-order hyperpolarizability (γ) of the material was determined using equation (6) [33]:

$$\gamma = \frac{I_m[\chi^{(3)}]}{f^4 C_{mol} N_A} \tag{6}$$

where N_A is the Avogadro constant as defined above, C is the concentration of the active species in the triplet state per mole, and f is the Lorentz local field factor given as $f = (n^2 + 2)/3$.

3. Results and discussion

3.1. *Characterization of Pc complexes*

Each of the pyrene-derivatized phthalocyanines, **3** or **4** was prepared according to the reaction pathway shown in scheme 1. The compounds were characterized with spectroscopic techniques such as the UV−vis, MALDI-TOF MS, IR, ^{1}H NMR, and elemental analysis. The complete disappearance of the –NH_2 vibrations at 3337 and 3233 cm^{-1} [10] in **3** clearly indicates the successful conversion of the four terminal amino groups in **1** to imine functionalities. For the asymmetric **4**, a weak broad band at ~3206 cm^{-1} may be attributed to the vibrational band of the only single terminal amino group in the molecule. Furthermore, the appearance of imine bands at 1668 and 1670 cm^{-1} in the final products **3** and **4**, respectively [34], clearly indicate the formation of the target compounds.

The ^{1}H NMR spectra of **3** and **4** in deuterated DMSO solution were observed as multiplets for the phenoxy protons between 7.00–8.25 and 7.11–7.87 ppm, respectively, which on integrating gave 16 protons. The proton signals of the Pc rings for **3** and **4** were

observed between 7.50–8.78 and 7.41–8.53 ppm, respectively, as multiplets, and which on integrating gave 12 protons. The pyrene protons were observed between 8.63–8.90 for **3** and 8.23–8.75 ppm for **4**, giving 36 and 27 protons, respectively, on integrating. A broad singlet integrating for 4 and 3 protons, respectively, was observed for **3** and **4** and is attributed to the imine protons at 8.93−8.98 and 8.67–8.70 ppm, respectively. A broad singlet attributed to the $-NH_2$ protons around 6.36–6.42 was observed in **4**. On addition of a small amount of D_2O to the sample, the $-NH_2$ protons for **4** were rapidly exchanged with the added D_2O, resulting in the disappearance of this peak from the spectrum, and thus confirming the assignment of this peak to the $-NH_2$ signal. In the mass spectra of **3** and **4**, *m*/*z* at 1936 and 1730 were observed, corresponding to $[M-2H]^+$ and $[M+2H]^+$ molecular ions, respectively. MPc complexes have been observed to fragment with molecular ion peaks $[M]^+$, $[M+nH]^+$ or $[M-nH]^+$ [35], hence the observed mass spectral data. The measured C, H, and N elemental data are consistent with hydrated Pcs, with **3** and **4** found to contain 6 and 4 molecules of water, respectively. The measured elemental results are in agreement with observations in the chemical literature that Pcs are often isolated as hydrates [36], hence, confirming the purity of the final products.

The electronic absorption spectra of **3** and **4** are presented in figure 1. Typical of MPcs, the characteristic Q-bands and B-bands were observed. The Q-bands of **3** and **4** were observed at 697 and 699 nm, respectively (table 1). The B-band of **3** is almost as intense as its Q-band because of the pyrene absorption in the B-band region (figure 1). Complex **3** has more pyrene groups than **4**, hence, has a more intense B-band absorption. The complexes obeyed Beer's law for concentrations ranging from 1×10^{-7} to 1×10^{-5}, confirming lack of aggregation.

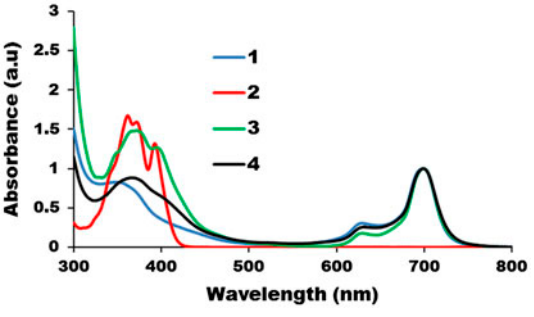

Figure 1. Electronic absorption spectra of **3** (green) and **4** (black) in DMSO, conc. $\approx 1.0\times10^{-5}$ M. Overlaid on the graph are the starting Pc, **1** in DMSO (blue) and the pyrene, **2** in ethanol (red) (see http://dx.doi.org/10.1080/00958972.2014.959509 for color version).

Table 1. Properties of **3** and **4** in DMSO at room temperature in comparison with some photophysical properties of **1**. Excitation λ for fluorescence emission studies = 610 nm. τ_F were determined at the emission maxima.

Compound	$\lambda_{Q\text{-band}}$ (nm)	τ_F (ns)	$\tau_{F(av)}$ (ns)	Φ_T	τ_T (μs)	$\tau_{ISC(av)}$ (ns)	Φ_{IC}
3	697	3.71 ± 0.15 (1.1%) 0.23 ± 0.01 (98.9%)	0.27 ± 0.06	0.79	83	0.34 ± 0.08	~0.21
4	699	3.16 ± 0.12 (1.2%) 0.23 ± 0.01 (98.8%)	0.26 ± 0.05	0.83	85	0.31 ± 0.08	~0.17
1[a]	698	0.29 ± 0.01 (55.2%) 2.91 ± 0.04 (44.8%)	1.46 ± 0.05	0.72	52	2.03 ± 0.03	~0.28

[a]Data from Ref. [10].

3.2. *Photophysical properties*

The heavy atom effect promotes ISC to the triplet manifold, hence discouraging fluorescence and promoting the population of the triplet state [37]. The low fluorescence quantum yields (Φ_F) for **3** and **4** (<0.01 in both samples) are typical of Pcs with heavy atom centers, such as InPcs [10, 16, 38]. The fluorescence decay times (τ_F) from TCSPC were determined by fitting the luminescence decay data to a biexponential function (table 1). The presence of two lifetimes in phthalocyanines has been explained in terms of the presence of aggregates which quench fluorescence resulting in quenched and unquenched fluorescence [39]. The quenched fluorescence lifetimes were in higher abundance.

The high triplet yields (Φ_T) obtained for **3** and **4**, 0.79 and 0.83, respectively (table 1), showed evidence of the enhancement of triplet absorption by the presence of pyrene units when compared to MPcs in general [40]. As shown in table 1, the values obtained for **3** and **4** are larger than for **1**. Thus pyrene promotes population of the triplet state. The higher Φ_T value of **4** relative to **3** may well be explained using the concept of symmetry. Previous reports [19] have shown that less symmetric Pc molecules show higher excited triplet absorption. The triplet lifetimes τ_T obtained for these molecules, 83 and 85 μs for **3** and **4**, respectively (table 1), are short, corresponding to the observed high triplet quantum yields [41]. The lifetimes are however improved for **3** and **4** compared to **1** (table 1). Thus, pyrene improves both the triplet state quantum yields and lifetimes. Similarly, the ISC times (τ_{ISC}) estimated using the equation $\tau_{ISC} = \tau_F/\Phi_T$ [42] decreased with increasing triplet yields as expected (table 1), thus showing that the transitions from the excited singlet state to the triplet state is faster in **4** than **3**, which corroborate the observed triplet data.

The quantum yields of internal conversion (Φ_{IC}) obtained from the equation $\Phi_{IC} = 1 - (\Phi_F + \Phi_T)$ are summarized in table 1. This equation assumes that only three processes (fluorescence, ISC, and internal conversion) jointly deactivate the excited singlet states of the complexes. More energy was lost via internal conversion in **3** than in **4**, judging by the higher yield of internal conversion (Φ_{IC}) of ~0.21 for **3** compared to ~0.17 in **4** (table 1).

3.3. *Nonlinear optical parameters*

3.3.1. 2PA (β_2) coefficients and cross-sections (σ_2). Figure 2A shows the representative open-aperture *Z*-scans of **3** and **4** obtained at 532 nm using 10 ns pulses. Absorbance of the samples was kept at ~1.5, corresponding to ~1.04×10^{-5} M of **3** and ~1.20×10^{-5} M of **4** in DMSO. The on-axis peak input intensity was ca. 310 MW cm^{-2} for each measurement. Measurements for each sample were done in triplicate, and the reported 2PA coefficients (β_2) are the average. All measurements revealed strong nonlinear absorption (NLA) behaviors in both samples, with the shapes of the *Z*-scan profile exhibiting reverse saturable absorption (RSA) signature [28]. Analyses of the *Z*-scan results to obtain β_2 were done by fitting the data to the 2PA function described above, equation (1). The representative fitting plot is shown in figure 2B. Further analyses to obtain the other NLO parameters were carried out using the methods described in the literature [30–33]. The results of the measurements are summarized in table 2.

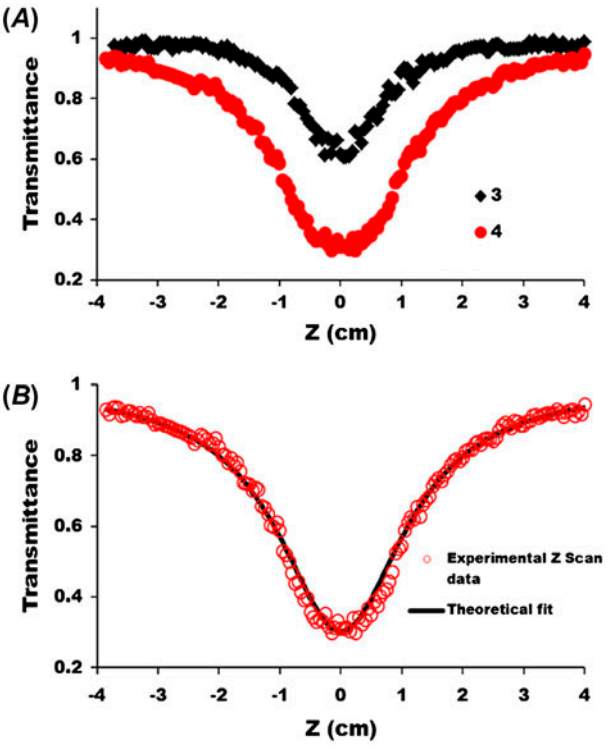

Figure 2. (A) Representative open-aperture Z-scan signatures of the investigated compounds at absorbance of 1.5, i.e. ([**3**] ≈ 1.04 × 10^{-5} M, [**4**] ≈ 1.20 × 10^{-5} M). Peak input intensity (I_{00}) ≈ 310 MW cm^{-2}. (B) Open-aperture Z-scan for the solution of **4** in DMSO showing the fitting. The black solid curve is the theoretical fit.

The measured β_2 values for **3** and **4** were 9.9 cm GW^{-1} and 53.8 cm GW^{-1}, respectively (table 2). We have earlier reported for **1** in DMSO, a much higher NLA coefficient of 221.6 cm GW^{-1} at ~260 MW cm^{-2} [10] (table 2). However, the Φ_T value reported for this molecule was lower compared to those of **3** and **4** as shown in table 1. These results were not expected since it is generally believed that increase in triplet-state populations should lead to improved NLO properties [43]. To explain this observation, we obtained at varying on-focus peak intensities (I_{00}), a series of β_2 values. The measured β_2 were then plotted against the corresponding I_{00} (figure 3A). The plot showed an exponential decrease in β_2 with increasing I_{00}. Interestingly, at a much lower I_{00} of ~137 MW cm^{-2}, ~223 cm GW^{-1} and ~273 cm GW^{-1} β_2 values were obtained for **3** and **4**, respectively. These values are higher than 221.6 cm GW^{-1} earlier reported for **1** at ~260 MW cm^{-2} [10]. At a higher I_{00} of ~302 MW cm^{-2}, the measured β_2 values dropped drastically to ~20.65 cm GW^{-1} and ~65.87 cm GW^{-1} for **3** and **4**, respectively. The trend observed in **3** and **4** may be explained on account of an increase in the rate of depletion of two-photon absorbers (2PAs) in the triplet state, as the on-focus intensity increases. Therefore, we assume for these complexes, a continuous increase in the rate of depletion of 2PAs from the S_0 state by *linear absorption* process to the S_1 state as I_{00} increases. The instantaneous depletion rate of **1** is thus assumed to be less than those of **3** and **4**. This assumption may be justified by the $\tau_{F(av)}$ values recorded for the studied compounds (~0.26 ns), table 1, which are shorter than 1.46 ns

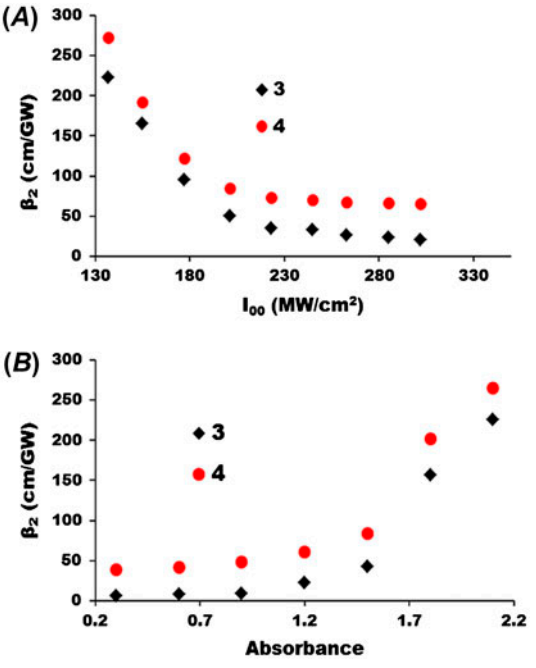

Figure 3. Plots showing the (A) peak intensity (I_{00}) dependence of β_2 and (B) the concentration (absorbance) dependence of β_2 for the two Pcs (**3** and **4**) in DMSO. Each data point represents an independent open-aperture *Z*-scan in A and B. Absorbance = 1.5 for each sample in A. Peak intensity (I_{00}) ≈ 310 MW cm^{-2} for each independent measurement in B.

Table 2. Nonlinear optical properties of **3** and **4** in DMSO at an absorbance of 1.5 A. All data were obtained by pumping 10 ns pulses at 532 nm wavelength. The peak intensity for each measurement was ≈310 MW cm^{-2}.

Compound	β_2 (cm GW^{-1})	$I_m[\chi^{(3)}]$ (esu)	γ (esu)	σ_2 (cm^4 s photon^{-1})	$g^{(2)}$ (%)	I_{lim} (J cm^{-2})
1[a]	221.6	7.80×10^{-11}	3.90×10^{-27}	–		0.28
3	9.9	3.49×10^{-12}	2.63×10^{-28}	7.40×10^{-43}	8.4	2.93
4	53.8	1.89×10^{-11}	1.02×10^{-27}	2.89×10^{-42}	9.1	0.54

[a]Data from Ref. [10].

reported for **1**. The implication of this is that **3** or **4** spent less time in the S_1 state compared to **1** (higher S_1 depletion rates in **3** and **4** were observed), before undergoing a spin forbidden transition to the excited triplet state where they got depleted by a different process known as *nonlinear absorption*.

Similarly, a plot of β_2 *versus* the sample concentration (absorbance) showed an exponential increase in β_2 with increasing absorbance values (figure 3B). We have earlier reported for a series of lead pyridyloxy Pcs, the dependence of β_2 on the number of statistically available 2PAs in the excited state [16], with the resultant effect being an increase in the 2PA cross-section (σ_2) as the sample concentration increases. For the molecules under investigation (**3** and **4**), the observed NLA is also predominantly dependent on the number of the available 2PAs.

The two important analyses for confirming a 2PA-dependent RSA are shown in figure 4. An exponential decrease in transmittance with increasing input fluence (I_0) is characteristic of a 2PA induced RSA [44, 45]. In figure 4A, **3** showed a negative linear curve devoid of any region of saturation. This observation is different from the commonly observed exponential decrease in transmittance with increasing I_0 as observed here for **4** and the previous literature reports [16, 44, 45]. Since both samples showed similar ISC time (τ_{ISC}) to the triplet state, it is expected that both would show similar NLA behavior. An τ_{ISC} that is

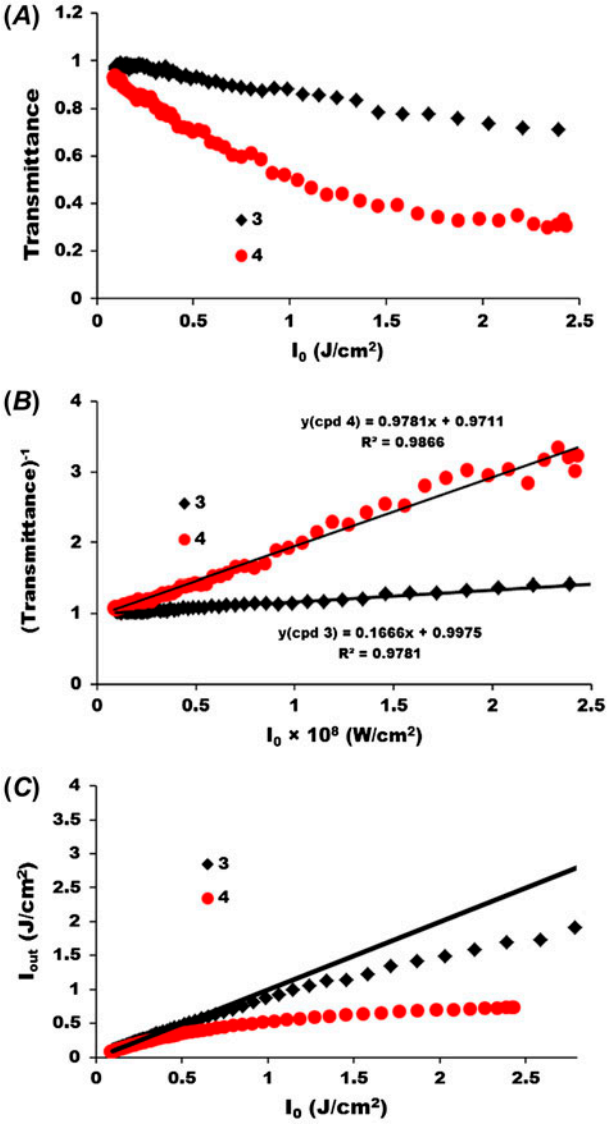

Figure 4. (A) Transmittance *vs.* input fluence (I_0) curves for **3** and **4**. (B) Intensity-dependent transmission of **3** and **4**. (C) Output fluence (I_{out}) *vs.* input fluence (I_0) curves for **3** and **4**. All measurements were taken at 1.5 absorbance and $I_{00} \sim 310$ MW cm^{-2}.

much less than the pulse duration of the laser system employed, i.e. $\tau_{ISC} \ll 10$ ns (table 1), as is the case for **3** and **4**, should promote efficient ISC to the triplet state.

A good fit obtained for the two samples with equation (3) (figure 4B) further confirms the dependence of the observed RSA on a 2PA mechanism. The smaller slope obtained for **3** also suggests that the excited state is sparsely populated by two-photon absorbers, unlike **4** with a relatively bigger slope, which implies a larger population of the two-photon absorbers in the excited triplet state. Another important parameter from equation (3) is the $g^{(2)}$ value, which may be interpreted as the degree to which other processes apart from the speculated 2PA have contributed to the observed NLO is presented in table 2; $g^{(2)}$ values of 8.4% and 9.1% were found, respectively, for **3** and **4**. The measured σ_2, 7.40×10^{-43} for **3** and 2.89×10^{-42} for **4** (in units of $cm^4\,s\,photon^{-1}$) are within the range of the reported values for most organic-based nonlinear optical materials [30]. However, it is worth noting that the observed σ_2 for **3** and **4** are greater than those reported for polymer matrices of 2,5-benzothiazole-3,4-didecyloxy thiophene [44], 4-[*p*-(*N*-ethyl-*N*-hydroxyethylamino)styryl]-*N*-methylpyridinium tetraphenylborate [45], and stilbene-based dyes [30] by three to four orders of magnitude, hence showing the importance of the pyrene units. It thus appears that the presence of the highly aromatic pyrene units in these molecules enhance the dipole moment vector which causes increase in the NLA at relatively lower incident energy. We expect the NLA performance to be much less, if the phenyl analogs of these pyrene derivatives are investigated under similar experimental conditions since they are less aromatic. The increase observed in β_2 of **3** and **4** (when compared to **1**) at a higher absorbance is due to increase in the number of the statistically available 2PAs as mentioned above.

3.3.2. Second-order (γ) and third-order $I_m[\chi^{(3)}]$) nonlinearities. Several mechanisms giving rise to NLO responses can operate in a system. A small perturbation of the electronic distribution in a material as a response to the electric field of the incident light results in normal linear polarization. At high intensities, the electronic distribution no longer follows the applied field, resulting in both second- and third-order nonlinearities. The estimated γ and $(I_m[\chi^{(3)}])$ values for the samples are given in table 2. In general, the values of γ and $(I_m[\chi^{(3)}])$ vary as expected in the same trend as the measured 2PA coefficients (β_2). The larger the value of γ, the better is the molecule as a nonlinear optical material. The absence of symmetry induces a dipole moment within the molecule. The larger the dipole moment within a molecule, the larger the γ value as observed for the asymmetric compound **4**, when compared to its tetra-substituted derivative **3**. The imaginary component of the third-order nonlinear susceptibility $(I_m[\chi^{(3)}])$ values estimated for the complexes are presented in table 2. These values are required to be sufficiently large as they determine the fastness of an optical material in responding to the perturbation initiated by an intense laser beam. The values obtained in this study are within the range of the previously reported values for most phthalocyanine-based nonlinear optical materials [29].

3.3.3. Optical limiting threshold. Optical limiting is an important application of nonlinear optics, useful for the protection of human eyes and sensitive optical equipment from intense laser beams. An important parameter in optical limiting measurement is the limiting threshold intensity or fluence (I_{lim}). It may be defined as the input fluence (or energy) at which the nonlinear transmittance is 50% of the linear transmittance [46]. The lower the I_{lim} value, the better is the material as an optical limiter. A good optical limiter must strongly attenuate

high intensity and potentially damaging light (such as focused laser beams), while still allowing high transmission of ambient light. The optical limiting curves obtained for the studied samples at an absorbance of 1.5 and ca. 310 MW cm^{-2}, I_{00} are presented in figure 4C. The relatively weak NLA behavior of **3** can be seen in the I_{out} *versus* I_0 curve, where the slope prior to the critical point is only slightly bigger than the slope after it, which thus results in output fluence not clamped at a constant value after the abrupt change. At 310 MW cm^{-2} value of I_{00}, the estimated I_{lim} value was high, ~2.93 J cm^{-2}. At the same I_{00}, **4** showed greater clamping of the output fluence to a relatively constant value compared to **3**. The estimated I_{lim} value for **4** was ~0.54 J cm^{-2}, which falls within the range of the previously reported values for most phthalocyanine-based optical limiters [19, 47]. Complex **1** however shows a smaller I_{lim} compared to **3** and **4**, but at a lower input fluence.

4. Conclusion

The photophysical and 2PA-dependent optical limiting properties of two indium(III) phthlocyanines bearing pyrene appendages have been investigated. The new molecules, tetra-substituted-**3**, and tri-substituted-**4**, with pyrene moieties showed faster ISC rate to the excited triplet manifold with increased triplet yields and lifetimes compared to the previously reported values for **1**, i.e. 2(3),9(10),16(17),23(24)-tetrakis-(4-aminophenoxy)phthalocyaninato indium(III) chloride. At lower on-focus beam intensities, the NLO response of the samples was more efficient than at higher intensities. However, increase in the sample concentration was found to increase the NLO behavior exponentially. The two molecules (**3** and **4**) showed similar relationship between the β_2 values and the sample concentration. The measured 2PA cross-section, second-order hyperpolarizability and third-order susceptibility values are within the range of earlier reported values for phthalocyanines, hence, making them important molecules for consideration in a broad range of photonics and optoelectronics applications.

Acknowledgement

KS thanks the African Laser Centre for a scholarship.

Funding

This work was supported by the African Laser Centre (ALC), the Department of Science and Technology (DST), CSIR National Laser Centre, Rental Pool Programme, National Research Foundation (NRF) of South Africa through DST/NRF South African Research Chairs Initiative for Professor of Medicinal Chemistry and Nanotechnology, and Rhodes University.

References

[1] K. Keis, J. Lindgren, S.-E. Lindquist, A. Hagfeldt. *Langmuir*, **16**, 4688 (2000).
[2] R.K. Pandey. *J. Porphyrins Phthalocyanines*, **4**, 368 (2000).
[3] T. Nyokong. In *N4-Macrocyclic Metal Complexes*, J.H. Zagal, F. Bedioui, J.-P. Dodelet (Eds), pp. 315–362, Springer, New York (2006).
[4] O. Adegoke, T. Nyokong. *J. Photochem. Photobiol., A*, **265**, 58 (2013).

[5] O. Adegoke, T. Nyokong. *J. Lumin.*, **146**, 275 (2014).
[6] M. Hanack, D. Dini, M. Barthel, S. Vagin. *Chem. Rec.*, **2**, 129 (2002).
[7] Y. Chen, L. Gao, M. Feng, L. Gu, N. He, J. Wang, Y. Araki, W.J. Blau, O. Ito. *Mini-Rev. Org. Chem.*, **6**, 55 (2009).
[8] A. Vicek Jr. *Coord. Chem. Rev.*, **200–202**, 933 (2000).
[9] S.-S. Sun, A.J. Lees. *Coord. Chem. Rev.*, **230**, 171 (2002).
[10] K. Sanusi, E.K. Amuhaya, T. Nyokong. *J. Phys. Chem. C*, **118**, 7057 (2014).
[11] S. Sürgün, Y. Arslanoğlu, E. Hamuryudan. *Dyes Pigm.*, **100**, 32 (2014).
[12] J. Bartelmess, B. Ballesteros, G. de la Torre, D. Kiessling, S. Campidelli, M. Prato, T. Torres, D.M. Guldi. *J. Am. Chem. Soc.*, **132**, 16202 (2010).
[13] R.O. Ogbodu, E. Antunes, T. Nyokong. *Dalton Trans.*, **42**, 10769 (2013).
[14] E.M. Maya, C. García, E.M. García-Frutos, P. Vázquez, T. Torres. *J. Org. Chem.*, **65**, 2733 (2000).
[15] G. de la Torre, P. Vázquez, F. Agulló-López, T. Torres. *Chem. Rev.*, **104**, 3723 (2004).
[16] K. Sanusi, E. Antunes, T. Nyokong. *Dalton Trans.*, **43**, 999 (2013).
[17] I.V. Khudyakov, Y.A. Serebrennikov, N. Turro. *J. Chem. Rev.*, **93**, 537 (1993).
[18] J.S. Shirk, R.G.S. Pong, S.R. Flom, H. Heckmann, M. Hanack. *J. Phys. Chem. A*, **104**, 1438 (2000).
[19] M. Hanack, T. Schneider, M. Barthel, J.S. Shirk, S.R. Flom, R.G.S. Pong. *Coord. Chem. Rev.*, **219–221**, 235 (2001).
[20] N. Masilela, T. Nyokong. *J. Photochem. Photobiol., A*, **223**, 124 (2011).
[21] S. Fery-Forgues, D. Lavabre. *J. Chem. Educ.*, **76**, 1260 (1999).
[22] A. Ogunsipe, J.Y. Chen, T. Nyokong. *New J. Chem.*, **28**, 822 (2004).
[23] T.H. Tran-Thi, C. Desforge, C. Thiec. *J. Phys. Chem.*, **93**, 1226 (1989).
[24] P. Kubát, J. Mosinger. *J. Photochem. Photobiol., A*, **96**, 93 (1996).
[25] M. Sheik-bahae, A.A. Said, E.W. Van Stryland. *Opt. Lett.*, **14**, 955 (1989).
[26] M. Sheik-Bahae, A.A. Said, T. Wei, D.J. Hagan, E.W. Van Stryland. *IEEE J. Quant. Elect.*, **26**, 760 (1990).
[27] E.W. Van Stryland, M. Sheik-Bahae. In *Characterization Techniques and Tabulations for Organic Nonlinear Materials*, M.G. Kuzyk, C.W. Dirk (Eds), pp. 655–692, Marcel Dekker, New York (1998).
[28] R.L. Sutherland. *Handbook of Nonlinear Optics*, 2nd Edn, Marcel Dekker, New York (2003).
[29] R.S.S. Kumar, S.V. Rao, L. Giribabu, D.N. Rao. *Chem. Phys. Lett.*, **447**, 274 (2007).
[30] J.E. Ehrlich, X.L. Wu, I.-Y.S. Lee, Z.-Y. Hu, H. Röckel, S.R. Marder, J.W. Perry. *Opt. Lett.*, **22**, 1843 (1997).
[31] R. Loudon. In *The Quantum Theory of Light*., Oxford University Press, London (1973).
[32] E.M. García-Frutos, S.M. O'Flaherty, E.M. Maya, G. de la Torre, W. Blau, P. Vázquez, T. Torres. *J. Mater. Chem.*, **13**, 749 (2003).
[33] D. Dini, M. Hanack. In *The Porphyrin Handbook: Physical Properties of Phthalocyanine-based Materials*, K.M. Kadish, K.M. Smith, R. Guilard (Eds), Vol. 17, pp. 22–31, Academic Press, New York (2003).
[34] Z. Meić, G. Baranović. *J. Pure Appl. Chem.*, **61**, 2129 (1989).
[35] A.Y. Tolbin, V.E. Pushkarev, G.F. Nikitin, L.G. Tomilova. *Tetrahedron Lett.*, **50**, 4848 (2009).
[36] J. Rusanova, M. Pilkington, S. Decurtins. *Chem. Commun.*, **19**, 2236 (2002).
[37] E. Glimsdal, M. Carlsson, T. Kindahl, M. Lindgren, C. Lopes, B. Eliasson. *J. Phys. Chem. A*, **114**, 3431 (2010).
[38] M. Durmuş, T. Nyokong. *Polyhedron*, **26**, 3323 (2007).
[39] J.A. Lacey, D. Phillips. *Photochem. Photobiol. Sci.*, **1**, 378 (2002).
[40] T. Nyokong, E. Antunes. In *The Handbook of Porphyrin Science*, K.M. Kadish, K.M. Smith, R. Guilard (Eds), pp. 247–349, Academic Press, New York (2010).
[41] J.R. Darwent, P. Douglas, A. Harriman, G. Porter, M.-C. Richoux. *Coord. Chem. Rev.*, **44**, 83 (1982).
[42] L. De Boni, E. Piovesan, L. Gaffo, C.R. Mendonça. *J. Phys. Chem. A*, **112**, 6803 (2008).
[43] J.W. Perry, K. Mansour, S.R. Marder, K.J. Perry, D. Alvarez Jr., I. Choong. *Opt. Lett.*, **19**, 625 (1994).
[44] G.S. He, R. Gvishi, P.N. Prasad, B.A. Reinhardt. *Opt. Commun.*, **117**, 133 (1995).
[45] G.S. He, J.D. Bhawalkar, C.F. Zhao, P.N. Prasad. *Appl. Phys. Lett.*, **67**, 2433 (1995).
[46] Y. Chen, L. Gao, M. Feng, L. Gu, N. He, J. Wang, Y. Araki, W.J. Blau, O. Ito. *Mini-Rev. Org. Chem.*, **6**, 55 (2009).
[47] M. Yüksek, A. Elmali, M. Durmuş, H. Yaglioglu, H. Ünver, T. Nyokong. *J. Opt.*, **12**, 1 (2010).